Materials Research. 2023; 26(suppl. 1): e20230034
DOI: https://doi.org/10.1590/1980-5373-MR-2023-0034

Comparative Study of the Influence of Aging Time at 850 °C on the Electrochemical Behaviour of Two Cast Super Duplex Stainless Steel

A. L. S. Cruz[a,b], *H. M. L. F. de Lima*[a*], *A. R. V. Xavier*[a], *W. S. Araújo*[c], *M. Martins*[d]

[a]*Universidade Federal do Cariri, Centro de Ciência e Tecnologia, Rua Ten. Raimundo Rocha, 1639, Cidade Universitária, Juazeiro do Norte, CE, Brasil.*
[b]*Universidade Federal de São Carlos, Programa de Pós-Graduação em Ciência e Engenharia de Materiais, Rodovia Washington Luís, s/n, São Carlos, SP, Brasil.*
[c]*Universidade Federal do Ceará, Departamento de Engenharia Metalúrgica e Materiais, Av. Mister Hull, s/n, Pici, Fortaleza, CE, Brasil.*
[d]*Centro Universitário Salesiano São Paulo, Departamento de Engenharia Elétrica, Rua Dom Bosco, 100, Santa Catarina, Americana, SP, Brasil.*

Received: January 12, 2023; Revised: April 01, 2023; Accepted: May 21, 2023

Two cast superduplex stainless steels were aged at 850°C for different times. The effect of aging on the electrochemical behaviour and hardness of both steels has been investigated. A comparative study between the two steels was carried out considering the difference in chemical composition between the alloys, that is, the presence of copper and tungsten in the 6A steel. Corrosion resistance was evaluated by potentiodynamic polarization test, electrochemical impedance spectroscopy and Mott Schottky analysis. The results showed the beneficial effect of 0.99%pCu and 0.70%pW addition to the cast SDSS retarding the embrittlement of the 6A steel aged at 850°C for 10 hours. The characteristic mechanism of localized corrosion in the aged samples for both materials was the selective dissolution of the ferrite phase.

Keywords: *Super duplex stainless steel, Sigma phase, Electrochemical behaviour, Copper.*

1. Introduction

Energy, naval, petrochemical and nuclear industry sectors have their principal activities centralized in environments of extreme conditions of temperature, pressure, dissolved gases, chloride ion concentration and stress, which require materials with high mechanical and corrosion resistance[1-3]. Super duplex stainless steels (SDSS) are materials that provide a better response to the necessities of these sectors.

Among its main characteristics, SDSS presents a biphasic structure - formed proportionally by ferrite and austenite phases -, high toughness, good stress corrosion cracking in chloride environments, and values higher than 40 for the Pitting Corrosion Equivalent Number (PREN), which gives the material excellent resistance to this kind of localized corrosion[4]. PREN values are defined from alloy chemical composition, being for alloys with and without the addition of W respectively, PREN = %Cr + 3,3. (%Mo + 0,5. %W) + 16. (%N) and PREN = %Cr + %Mo + 16. (%N)[5,6].

Stainless steels (SS) possess high corrosion resistance, characteristic attributed to the protective effect of the passive film formed on their surface[7,8]. However, the corrosion resistance of SS is influenced by factors such as environment characteristics (presence of chloride ions, pH, temperature, dissolved gases, e. g.), chemical composition and thermal history of the alloy, superficial defects, and inclusions[9-12]. SS shows a composition rich in alloying elements, such as chromium, nickel, molybdenum, carbon, copper, titanium, and manganese. Therefore, when exposed to certain temperature ranges, precipitation of secondary phases can occur, modifying the expected properties of the material[13-16]. Among the secondary phases, sigma (σ) phase is the most important because of its considerable precipitation and the negative effect on the mechanical properties and corrosion resistance[13,16].

The precipitation of the sigma (σ) phase may occur in temperatures between 600°C and 1000°C, preferentially in regions of high energy, such as: ferritic (α/α) or ferritic-austenitic (α/γ) grain boundaries, grain boundary triple junctions and dislocation[17]. Also, it is possible its precipitation from the χ phase, this acting as a nucleus[18]. In steel A890 grade 6A, for instance, its formation was observed between 700°C and 940°C[1]. Sigma is a phase harmful to the performance of SDSS that presents high hardness and brittleness, currently associated with the reduction of toughness and a decline in the corrosion resistance of the material[19,20].

Growth of the sigma phase occurs through the consumption of ferrite phase, due to the small activation energy required for the diffusion of chromium and molybdenum, elements in which the sigma phase is rich. As a consequence of this, regions with depletion of these elements are generated adjacently at the sigma phase, which, especially in the case of chromium – passivating element -, means a passive film less stable and less protector.

Some duplex stainless steels count on adding 0.5–1.0 wt.% copper to improve their corrosion resistance. However, the conclusions about the effect of this element in chloride media still are controversial and unclear[21-25].

*e-mail: hillane.lima@ufca.edu.br

Furthermore, although much has been studied about the effect of the sigma phase on the corrosion resistance of stainless steels, little is known about the effect of the presence of copper in the steel on the precipitation of this phase.

Thus, this work aims to evaluate the effects of the addition of copper on the sigma precipitation, and its impact on the corrosion resistance of super duplex stainless steels ASTM A890/A890M grades 5A (0.3 wt.% Cu) and 6A (0.99 wt.% Cu). The steels were aged at 850°C for 10 minutes, 1 hour, and 10 hours. The corrosion resistance of the samples was evaluated by electrochemical tests of potentiodynamic polarization, electrochemical impedance spectroscopy (EIS) and Mott-Schottky analysis in 0.6 mol/L NaCl solution. The samples of both alloys in different conditions were characterized by optical microscopy (OM), scanning electron microscopy (SEM) and microhardness *Vickers.*

2. Experimental

The materials used were two cast Super Duplex Stainless Steels (SDSS) ASTM A890/A 890/M grades 5A and 6A. The chemical composition and their pitting resistance equivalent number (PREN) values are given in Table 1. The as-received alloys were cut by abrasive discs, solution annealed at 1200°C for 1 hour in a muffle furnace, followed by water quenching. This procedure ensures complete dissolution of the possible precipitates in the ferrite matrix and at α/γ interfaces. After solution treatment, some samples of both materials were aged at 850°C for 10 min, 1h, and 10h.

By optical microscopy (OM) the heat-treated samples had their microstructure investigated. The specimens for metallographic observations and Vickers microhardness (HV) tests were superficially abraded with silicon carbide papers up to 1200 mesh and then polished with diamond paste from 6 μm to 1 μm. Their microstructures were sequentially revealed using the Beraha reagent (80mL distilled water, 20mL HCl, and 1g of potassium metabisulfite). Hardness measurements were performed using the Vickers method to evaluate changes in hardness that may indirectly indicate precipitation of the sigma phase in both alloys and correlate them with the aging treatment time. Each specimen was tested with a 0.1 Kgf load for 10s, with ten measurements performed for each ferritic and austenitic phase.

Corrosion resistance of the heat-treated materials was evaluated by potentiodynamic polarization test, electrochemical impedance spectroscopy (EIS) and Mott-Schottky analysis in 0.6 mol/L NaCl solution at room temperature. These tests occurred in a conventional three-electrode system: the specimen analyzed as the working electrode, platinum (Pt) grid as the counter electrode and saturated KCl silver/silver chloride ($Ag(s)|AgCl(s)|Cl^-(KCl\ sat.)$) as the reference electrode. The working electrode was constructed using the samples embedded in epoxy resin with electrical contact established by a copper wire. Before electrochemical tests, the working electrodes were abraded with silicon carbide paper up to 600 mesh, degreased with alcohol, washed with distilled water and dried with hot air. The interface between sample and resin was isolated with transparent nail lacquer leaving an area of 0.5 cm^2 exposed to the test. The interface isolation prevents crevice corrosion during measurements.

The electrochemical tests were initiated after monitoring open circuit potential (OCP) for 3600 s, when potential approaches a nearly steady-state. Potentiodynamic polarization tests were performed at a scan rate of 1.0 mV/s from OCP until reaching a current density of 1.0 mA. By the end of the measurement, the surface of the specimen was observed by SEM. EIS was performed at the corrosion potential with a frequency range from 100 kHz to 2.5mHz with 7 points/decade, and a signal amplitude perturbation of 20 mV. Mott–Schottky analysis was performed at a frequency of 10 Hz using an excitation voltage of 10 mV. These measurements were conducted in potentiostat-galvanostat Autolab models PGSTAT302N and PGSTAT101 with NOVA® software support. Each experiment was conducted at least three times to ensure consistent data. All tests showed good reproducibility.

3. Results and Discussion

In order to determine the morphology and distribution of α and γ phases for different heat treatment conditions, the microstructure of SDSS 5A and 6A was revealed. Microstructural examinations were carried out using optical microscope as shown in Figure 1. The solubilized samples 5A and 6A present a typical duplex steel microstructure: austenite islands (bright phase) distributed in a ferritic matrix (dark phase). For the aging conditions at 850°C (for 10 minutes, 1 hour, and 10 hours), the appearance of brighter precipitates in the ferritic phase can be observed. The sigma phase occurs within or close to the ferrite grains due to its higher solubility of chromium and molybdenum[26], which are formers of the sigma phase. The sigma phase emerges from the phase transformation $\delta \rightarrow \sigma$ (ferrite to sigma phase) with precipitation of sigma phase in the high Cr-concentrated region of ferrite, being formed directly from this phase. The bright appearance after the attack is explained by the greater resistance of these precipitates to chemical attack, a consequence of the higher content of Cr present in this phase[27].

Sigma-phase precipitation is already observed for the shortest aging time (10 minutes) at 850°C in the microstructure of both alloys. The easy sigma phase precipitation is associated with the high Cr and Mo content in both alloys[1,28]. With increasing aging time at 850 °C, it was observed a greater tendency for sigma phase precipitation. This result is more pronounced for 5A steel, which can be attributed to the difference in chemical composition between the alloys.

Table 1. Chemical composition for the SDSS (wt.%) and their respective PREN values.

SDSS	C	Cr	Ni	Mn	Si	Mo	Cu	W	N	Fe	PREN
5A	0,028	25,51	7,84	0,96	0,75	4,25	0,30	-	0,229	Bal.	43,19
6A	0,029	26,11	8,23	0,72	0,88	3,63	0,99	0,70	0,221	Bal.	42,77

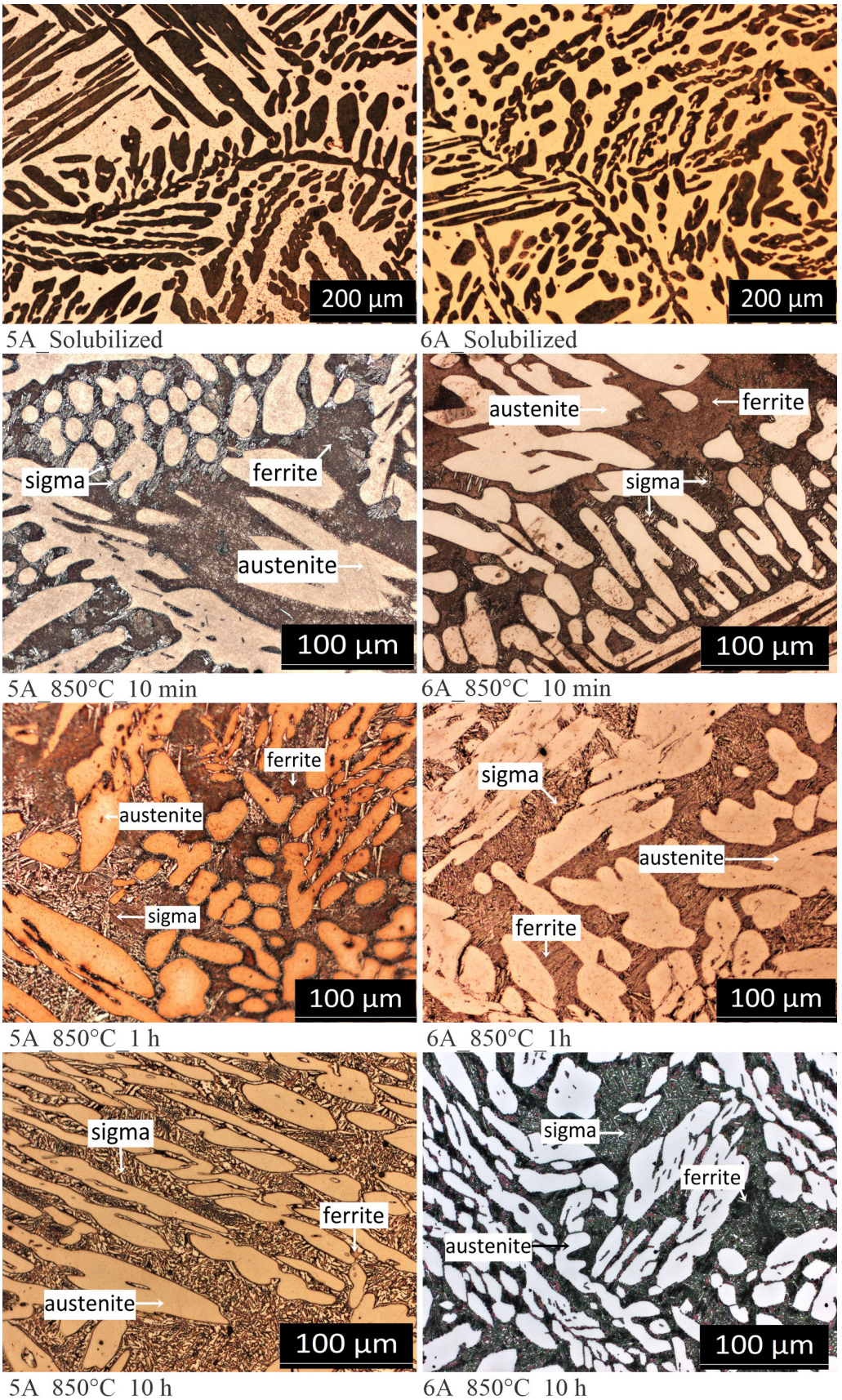

Figure 1. Optical micrographs of the microstructures of 5A and 6A steels.

This result it is possibly related to the higher copper content in this alloy. A similar result was observed by Wegrzyn and Klimpel[29]. The authors developed a study focused on the relationship between the addition of alloying elements Cu, W, V, Si, Nb, and the occurrence of the sigma phase, concluding especially on the retarding effect of Cu on the precipitation of this deleterious phase.

Vickers microhardness tests were carried out to verify indirectly the precipitation of the sigma phase and the effect of this phase on the hardness of the studied alloys. The results are shown in Figure 2. From the average microhardness values for the 5A and 6A steels, it is possible to notice that the samples in the aged condition showed higher hardness value for the ferrite phase than solubilized samples. Higher hardness values can be associated with the presence of the sigma phase, which is precipitated from within the grain of the ferrite phase and along the ferrite /austenite phase boundaries[30]. Relating hardness to treatment time, the relationship between these variables is precise, showing that longer aging times result in greater hardness, and, finally, greater sigma phase precipitation. Similar results were described by other studies[26,31]. Additionally, for the aged samples, the increase in hardness values of the ferrite phase was greater in steel 5A, confirming a lower formation of the sigma phase for the steel 6A observed in the metallographic analysis.

Figure 3 shows the cathodic and anodic potentiodynamic polarization curves of the two SDSS in different heat treatments conditions in 0.6 mol/L NaCl solution at room temperature. In all curves it was not observed the active-passive transition. The polarization curves indicate the electrochemical behaviour superior of the solubilized samples to the aged samples. In the solubilized condition the polarization curves of samples are characterized by a larger passivation region, starting around 100 mV extending to higher potential values (circa 1.0 V (vs. Ag(s)|AgCl(s)|Cl^-(KCl sat.)). Moreover, during the anodic scan the passive current density are very small, indicating greater stability and good protection efficiency of the passive film formed on the surface of the solubilized samples in the corrosion and passive potential domain. The increase in current observed at potentials close to 1.0 V may be linked to the anodic currents referring to the oxygen evolution on the surface of the material. This phenomenon causes an increase in current density, as a consequence of the generation of oxygen bubbles close to the surface, which facilitates the breaching of the passive film and the consequent nucleation of pits[32,33].

The polarization curves of samples heat treated at 850°C showed an instability in the passive region, peaks with low current density values and short duration, indicating nucleation of metastable pitting, and a reduction of that region[34]. Such behaviour can be justified by the presence of precipitates due to the aging of the samples. The presence of the sigma phase in the aged samples damage the stability of the passive film, since its precipitation results in poor adjacent regions in Cr and Mo[35]. This instability was not observed for the solubilized samples.

The pitting potential and current density data and their respective standard deviations obtained from the polarization curves are presented in Table 2. High potential values indicate lower susceptibility to pitting corrosion[36]. It is possible to observe that the aging at 850°C caused a reduction in the pit potential values of the samples compared to the solubilized condition samples. The two steels presented a similar behaviour between the samples aged for 10 min and 1 hour.

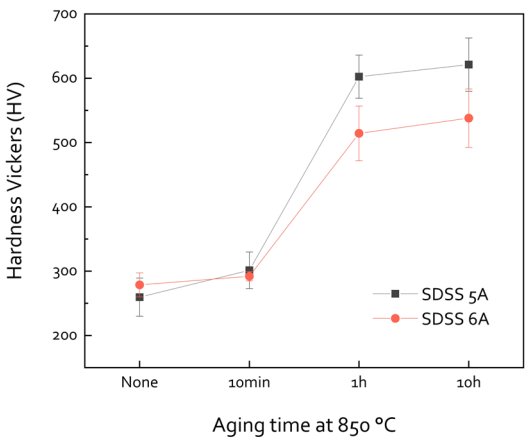

Figure 2. Microhardness values in ferritic regions of the samples of SDSS grade 5A and 6A, solubilized condition (none aging) and aging at 850°C for 10 minutes (10 min), 1 hour (1h), and 10 hours (10h).

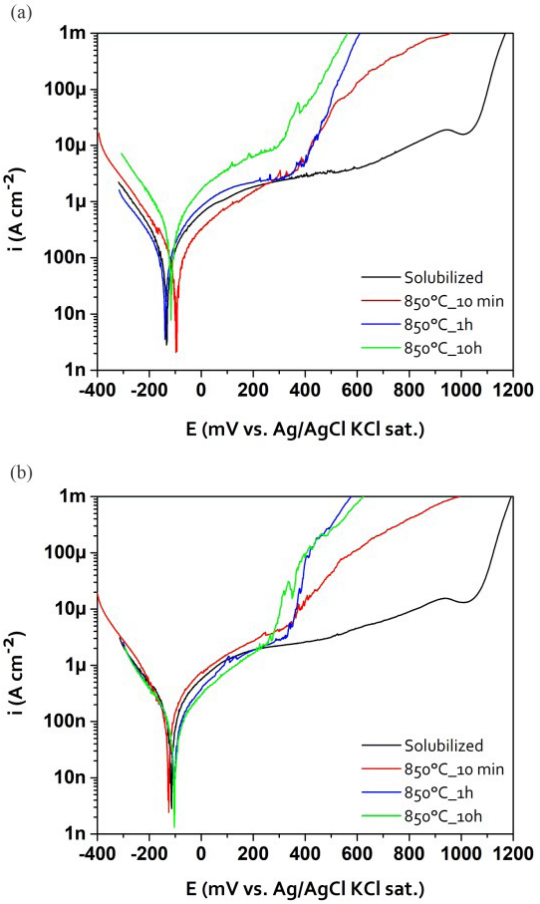

Figure 3. Potentiodynamic polarization curves of (a) 5A and (b) 6A SDSSs in 0.6 mol/L NaCl solution.

Furthermore, a more noble behaviour for the 5A steel was observed. However, the difference between the values obtained is small in each condition. This result shows that the addition of 0.99%pCu and 0.70%pW to the 6A steel doesn't seem to cause changes in the electrochemical behaviour during the initial stage of aging at 850°C for up to 1 h.

Increasing the aging time to 10 h, an increase in the values of current density in the passivation region for the 5A steel is observed. The superior behaviour of alloy 6A is associated to lower sigma phase precipitation, as observed in metallographic analysis and indirectly by hardness measurements. This result may be related to the addition of Cu and W in this steel. Copper and its role in the corrosion resistance of alloys is still a subject of much contradiction. However, several studies have demonstrated the beneficial effect of this element. Jeon et al.[37], in their studies with hyper duplex stainless steels (HDSS), report that additions of W to HDSS decrease the total amount of secondary phases when compared to the base alloy. This result suggests that the increase in W retards the precipitation of the secondary phases, especially sigma phase. In a complementary work about HDSS with the presence of W, Jeon et al.[38] studied the effect of Cu on the precipitation of secondary phases. The addition of Cu results in pronouncedly suppressing the fraction of the sigma phase.

At the end of the potentiodynamic polarization test, the surfaces of the samples were observed by SEM. The surface morphologies of the specimens in the solubilized condition and aged at 850°C after the linear polarization are shown in Figure 4 and 5. Dark spots observed on ferrite and austenite phases are non-metallic inclusions, present in both materials and typical of cast components[39]. Figure 5 shows the analysis for the solubilized samples. Secondary electron (SE) images show that non-metallic inclusions were preferential regions for the onset of localized corrosion. For samples under different aging conditions, images are shown in the backscattered (BSE) mode, from which it is possible to identify the different phases present in the material as shown in Figure 6. It was found that precipitates of sigma (σ) phase were formed in the specimens and that these precipitates formed continuous networks along the grain boundaries while also appearing randomly within the grains. Sigma (σ) phase appear lighter than ferrite and austenite because the higher Mo content increases the average atomic number (Z) and, thus, the backscattered electrons emission[40-42]. The inclusions, predominantly oxides, appear darker than ferrite and austenite in the SEM with BSE analysis, because the average atomic number (Z) is lower.

In the condition of aging at 850°C for 10 min, in both alloys, the presence of randomly distributed pits and pits nucleated preferentially from the inclusions was observed (Figure 5a-b).

Table 2. Pitting potential and current density data and their respective standard deviations obtained from the polarization curves in 0.6 mol/L NaCl solution.

Heat treatment condition	5A		6A	
	Pitting potential (V vs. Ag(s)|AgCl(s)|Cl^-(KCl sat.)	Current density (μA cm^{-2})	Pitting potential (V vs. Ag(s)|AgCl(s)|Cl^-(KCl sat.)	Current density (μA cm^{-2})
Solubilized	1.03 ± 0.01	21.9 ± 0.81	1.03 ± 0.01	17.9 ± 0.93
850°C_10min	0.43 ± 0.04	5.46 ± 0.60	0.34 ± 0.01	5.78 ± 0.75
850°C_1h	0.37 ± 0.02	3.61 ± 0.56	0.34 ± 0.01	4.55 ± 0.83
850°C_10h	0.30 ± 0.01	9.69 ± 0.78	0.32 ± 0.01	4.24 ± 1.30

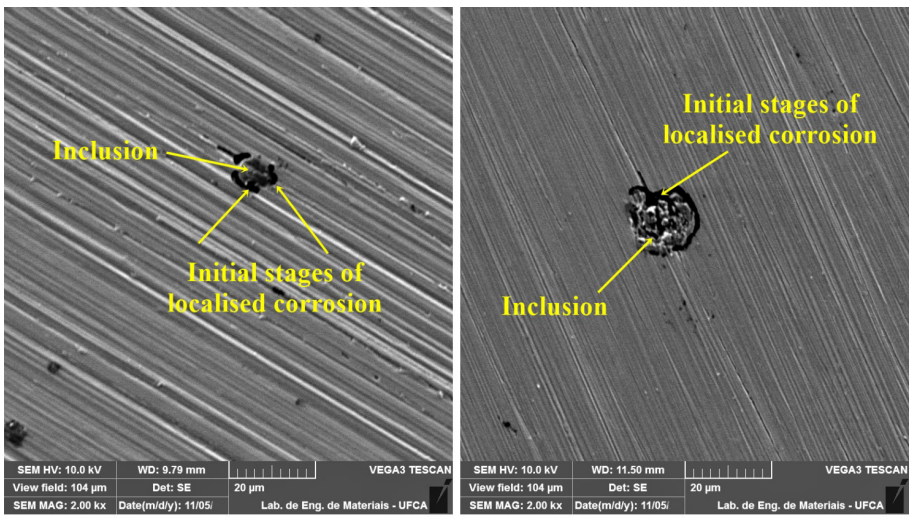

(a) (b)

Figure 4. SEM image of solubilized specimen after polarization test in 0.6 mol/L NaCl solution (a) 5A and (b) 6A SDSS.

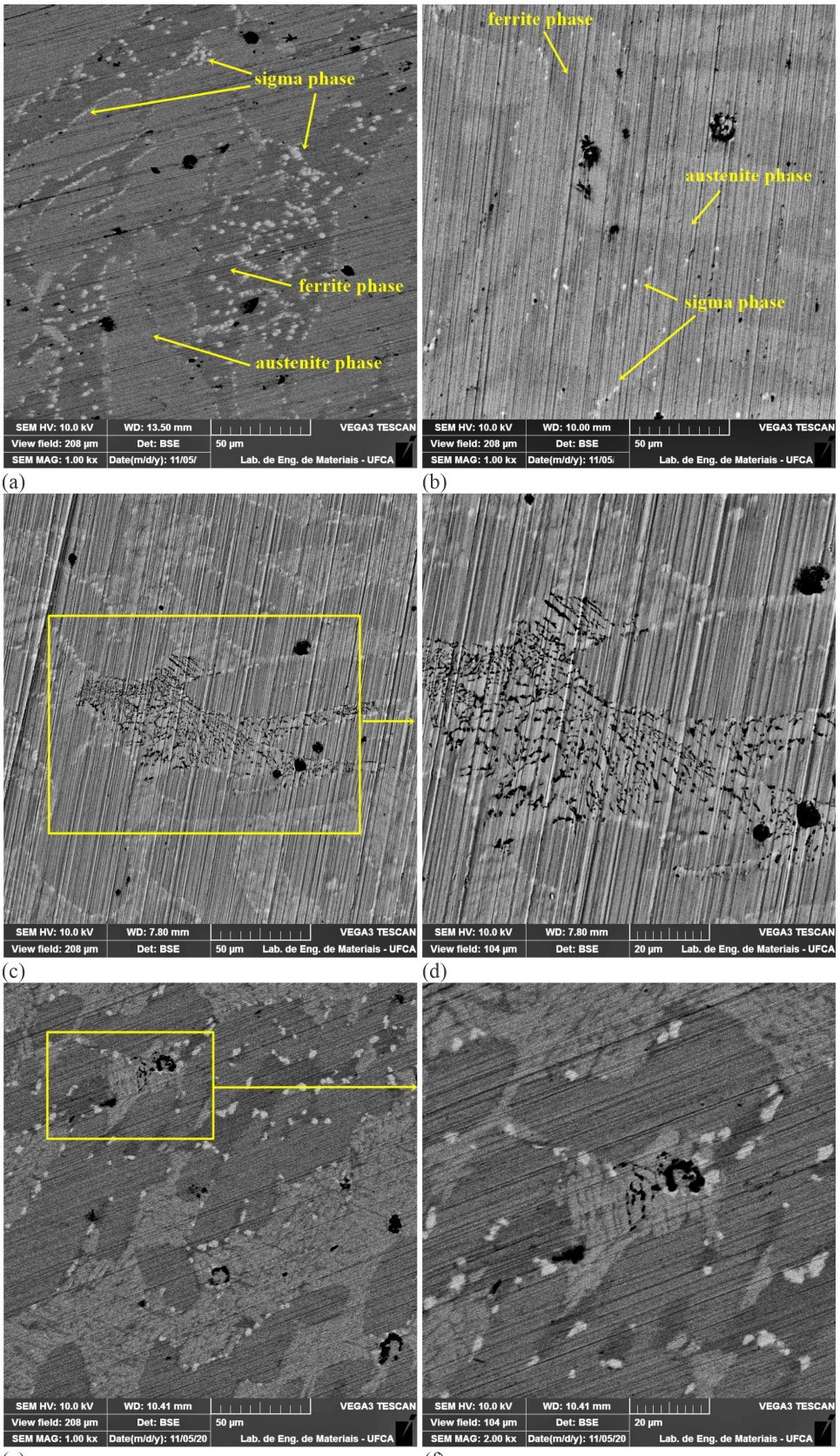

Figure 5. SEM image for aged samples at 850°C for 10 min (a) 5A and (b) 6A; for 1 h (c) 5A and (e) 6A; detailed SEM image of the selective attack of ferrite for aged samples for 1h (d) 5A and (e) 6A after linear polarization in 0.6 mol/L NaCl solution.

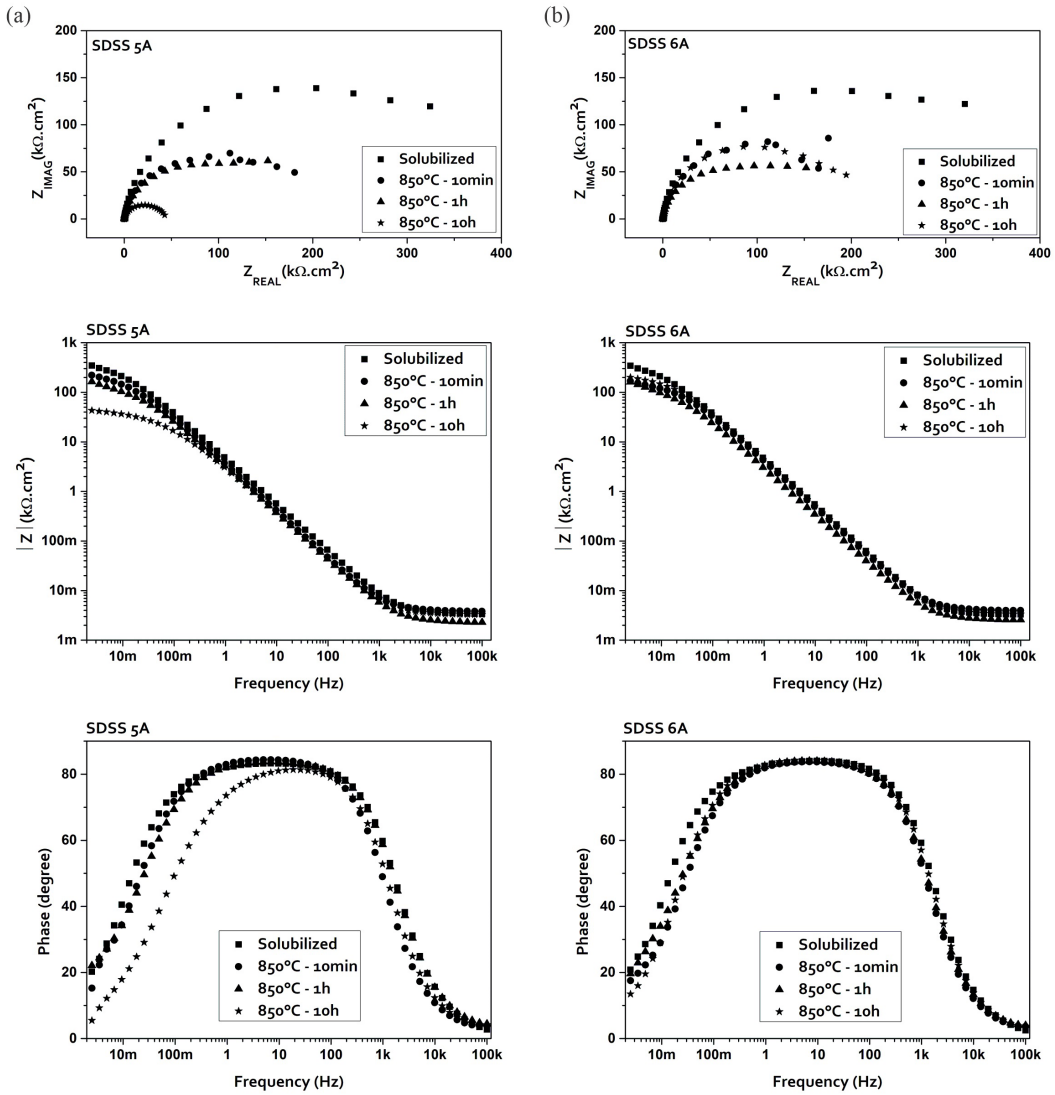

Figure 6. Nyquist and Bode plots for EIS data in 0.6 mol/L NaCl solution of specimens (a) 5A and (b) 6A.

By increasing the aging time to 1 h, a severe localized corrosion with numerous micropits distributed uniformly occurred within grain as well as along grain boundary in the ferrite phase, while the austenite phase was preserved and did not present significant dissolution as shown in Figure 5c and 5e. Figure 5d and 5f shows a more detailed SEM micrograph of the selective attack of the ferrite phase in the aged sample after the linear polarization test. Similar images were observed with increasing aging time to 10 h. This result shows that the lowest pitting potential observed in the polarization curves resulted from Cr and Mo-depletion occurred within the grain and along the grain boundary of the ferrite phase due to the precipitation of sigma phase already in the first minutes of aging at 850°C.

Electrochemical impedance spectroscopy was used to characterize the stainless steel/passive film/electrolyte interface at OCP. Figure 6 shows typical Nyquist and Bode plots obtained in 0.6 mol/L NaCl solution for SDSS 5A and 6A samples heat treated at 850°C for 10 min, 1h and 10h.

As can be seen from the figure, the Nyquist plots contain a depressed capacitive loop in the high frequency range. The capacitive loop observed in all diagrams can be attributed to the fast charge transfer reaction and the electrical double layer formed on the metal surface[43]. Since the charge-transfer resistance (i.e., corrosion resistance) is associated to the diameter of semicircles, the diameters of semicircles related to solubilized samples are bigger than those related to aged samples. Showing the harmful effect of aging at 850°C on corrosion resistance in both materials.

For 5A steel, the graph behaviour and the impedance values obtained for the samples aged at 850°C for 10 min and 1 hour were similar. As the aging time increases to 10 hours, there is a sharp drop in the impedance value, showing a deterioration in the protective capacity of the passive layer in this condition. This tendency is not observed for the 6A steel sample aged at 850°C for 10 hours, in this condition the Nyquist plots are compared with plots obtained for samples aged at 10 min.

The Bode-phase plots give one-time constant and a maximum phase angle close to 80° over a wide frequency range for all heat treatment condition. This evolution revealed the formation and growth of a passive film. The deviations of phase angle from 90° and of the slope in the impedance modulus plot expressed that the system did not behave like an ideal capacitor[44]. Therefore, in the studied frequency range, the (R(Q(R(QR))) equivalent electrical circuit (Figure 7) was proposed to fit and analyse the obtained EIS data. The selection of this circuit was based on EIS results and this model provides betters and accurate fitting values. In this model, the passive film is considered to have a porous structure and to show non-ideal capacitive behaviour. Rs is the electrolyte resistance, R_1 represents the product film resistance generated on the metal surface and R_2 is the charge transfer resistance[45]. Q_1 and Q_2 are constant phase elements (CPE), Q_1 is associated with capacitance generated by the oxide film on the electrode surface and Q_2 represents the double layer capacitance. CPE element is used to explain the depression of the capacitance semi-circle, which corresponds to surface heterogeneity. The impedance of the CPE was given by Brug et al.[46]: $Z_{CPE} = Y_0^{-1}(j\omega)^{-n}$. Where Y_0 are constants proportional to the capacitance of the passive film (magnitude of the CPE), j represents the imaginary unit, ω is the angular frequency, and n is the exponent ($-1 \leq n \leq 1$), which represents the divergence from ideal capacitance characteristics[47-49]. Results of the fitting parameters are summarized in Table 3. A good agreement between EEC predictions and experimental data with chi-square (χ^2) values around 10^{-3} can be observed.

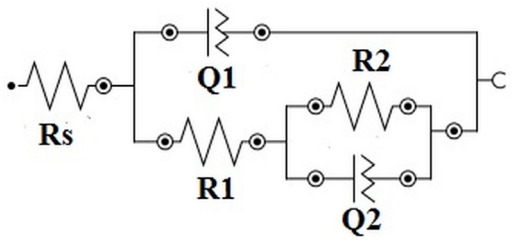

Figure 7. EEC used for fitting the experimental EIS data.

Table 3 shows that samples of steel 6A had higher values of R_1 and R_2 than samples of steel 5A under all heat treatment condition. Among the aged samples, it is possible to observe that for both materials studied, the values of R_1 and R_2 decrease with the aging time in the order 1 h > 10 min > 10 h. This tendency is more pronounced for the 5A steel, where a drastic reduction in the values of R_1 and R_2 is observed for the sample aged for 10 hours. This result shows the beneficial effect of addition of 0.99%pCu and 0.70%pW to the cast SDSS retarding the embrittlement of the steel, which may be associated with the delay in sigma phase precipitation for the 10 h aging condition.

It has been shown that the corrosion resistance of stainless steel was largely determined by the passive film semiconductor characteristics[50]. The electronic properties of passive films formed on SDSS 5A and 6A surface in 0.6 mol/L NaCl was studied based on the Mott-Schottky theory. The equation for Mott-Schottky analysis is[51]:

$$\frac{1}{C_{SC}^2} = \frac{2}{\varepsilon\varepsilon_0 q N_Q A^2}\left(E - E_{FB} - \frac{kT}{q}\right)$$ where C_{SC} is the space charge capacitance; ε_0 (= 8.854×10^{-14} F/cm) is the vacuum permittivity; ε (= 15.6) is the dielectric constant of the passive film[52]; Nq is the doping density; A is the sample area (cm^2); E_{FB} is the flat band potential; E is the applied electrode potential; k (=1.38×10^{-23} J/K) is the Boltzmann constant; q is the elementary charge (1.62×10^{-19} C) and T is the absolute temperature. The results are presented in Figure 8.

Two linear regions are observed in all Mott-Schottky plots. The sign of the slope is an indicator of the semiconductor type of the passive film. In the region below 0.5 V vs. Ag/AgCl (I) the slope is positive, and the films behave as n-type semiconductivity. In the region above 0.5 V vs. Ag/AgCl (II) the films behave as p-type semiconductor with negative slope. The zone near 0.5 V vs. Ag/AgCl occur an inversion from p-type to n-type semiconductor and is satisfied with flat condition. Such behaviour is associated with the existence of two layers, an outer iron-rich layer corresponding to n-semiconductivity and an inner chromium-rich layer corresponding to p-semiconductivity. The co-existence of n-type and p-type in the capacitance response was reported by Hakiki et al.[53] for oxide films on stainless steel. Furthermore, it is possible to observe that the capacitance response was lower for the 6A steel.

Table 3. Impedance parameters of the SDSSs 5A and 6A in 0.6 mol/L NaCl solution.

SAMPLE	R_s Ω.cm^2	CPE 1		R_1 kΩ.cm^2	R_2 kΩ.cm^2	CPE 2		χ^2
		Y_0 μF/cm^2	N1			Y_0 μF/cm^2	N2	
5A_Solubilized	17.55 ± 0.07	7.59 ± 0.12	0.93 ± 0.04	1273.0 ± 4.7	604.5.0 ± 0.70	35.35 ± 4.17	0.95 ± 0.07	0.003
5A_850°C_10min	11.1 ± 0.07	16.75 ± 1.34	0.95 ± 0.01	442 ± 0.10	227.0 ± 0.36	37.3 ± 3.11	0.91 ± 0.01	0.0006
5A_850°C_1h	13.8 ± 0.63	12.6 ± 0.70	0.93 ± 0.01	687.0 ± 36.7	609.0 ± 3.53	18.8.0 ± 7.4	0.97 ± 0.01	0.001
5A_850°C_10h	18.0 ± 0.08	16.5 ± 1.45	0.92 ± 0.01	119.0 ± 0.9	56.3.0 ± 14.4	15.0 ± 3.1	0.91 ± 0.02	0.005
SAMPLE	R_s Ω.cm^2	CPE 1		R_1 kΩ.cm^2	R_2 kΩ.cm^2	CPE 2		χ^2
		Y_0 μF/cm^2	N1			Y_0 μF/cm^2	N2	
6A_Solubilized	17.6 ± 0.26	7.3 ± 0.73	0.93 ± 0.01	1468.0 ± 3.5	606.0 ± 0.66	53.8 ± 3.4	0.98 ± 0.06	0.0001
6A_850°C_10min	15.35 ± 0.34	17.7 ± 5.6	0.93 ± 0.06	513.0 ± 11.24	397.0 ± 14.77	36.4.0 ± 5.23	0.96 ± 0.01	0.009
6A_850°C_1h	18.0 ± 0.60	9.07 ± 6.3	0.93 ± 0.01	709.2 ± 27.6	604.0 ± 29.27	25.9.0 ± 2.8	0.95 ± 0.01	0.005
6A_850°C_10h	15.4 ± 0.70	9.27 ± 0.36	0.94 ± 0.01	584.7 ± 11.95	243.0 ± 3.88	32.1 ± 2.4	0.90 ± 0.01	0.001

Table 4. Doping densities for passive films formed on SDSS 5A and 6A.

CONDITION	6A		5A	
	N_D (10^{21} cm^{-3})	N_A (10^{21} cm^{-3})	N_D (10^{21} cm^{-3})	N_A (10^{21} cm^{-3})
Solubilized	1.67 ± 0.22	1.45 ± 0.11	1.74 ± 0.09	1.57 ± 0.04
850°C_10min	1.81 ± 0.24	1.31 ± 0.07	1.93 ± 0.01	1.74 ± 0.12
850°C_1h	1.75 ± 0.11	1.38 ± 0.03	1.89 ± 0.10	1.42 ± 0.04
850°C_10h	2.11 ± 0.24	1.72 ± 0.24	2.61 ± 0.51	1.81 ± 0.20

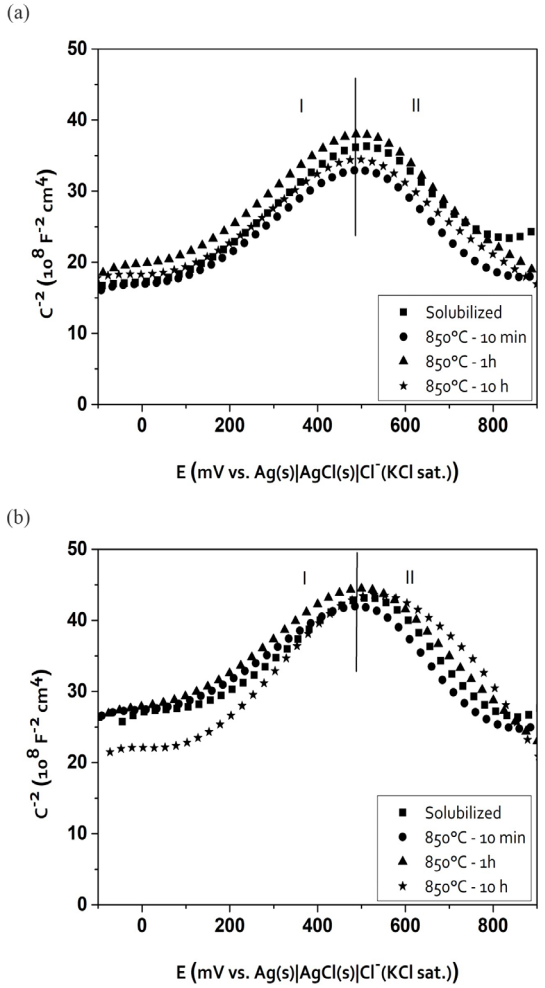

Figure 8. Mott-Schottky type plots of passive layers on cast DSS (a) 5A and (b) 6A in 0.6 mol/L NaCl solution.

The high capacitance response observed for steel 5A is associated with an increasing hole concentration in the valence band and an increase in the carrier density, which can be negative to the stability of the passive film[23].

N_A and N_D (acceptor and donor densities, respectively) can be calculated from the slopes of the experimental $1/C^2$ vs. E plots. Table 4 shows the calculated doping densities for the films formed on the surface of the studied alloys. The films present high doping densities in the range 10^{21} cm^{-3}, revealing a high conductivity comparable to those reported in other studies[53,54].

For both 5A and 6A steel, the doping density is lower for the sample in the solubilized condition than for the aged samples. Among the aged samples, the donor and acceptor densities decrease with aging time in the order 1 h > 10 min > 10 h.

Comparing the two steels, it is observed that in all heat treatment conditions the donor and acceptor densities for the 6A steel are lower than those observed for the 5A steel. The number of charge carriers is associated with the number of points defects[53,54]. The excess of vacancies is to be expected in the space charge region developed at the steel/Cr_2O_3 interface, and in the space charge region at the γ-Fe_2O_3/electrolyte n-type interface, an electron-depleted zone may be formed[55,56]. In this way, the greater the amount of charge carriers, the greater the presence of defects in the passive film, increasing the risk of passive film breakdown and pitting corrosion development.

The results of the Mott-Schottky analysis show that the addition of 0.99%pCu and 0.70%pW to the SDSS cast improved the structural quality of the passive film and therefore its stability and ability to protect against aggressive agents in the chloride medium. Additionally, it is possible to conclude that the protective capacity of the passive film formed in both steels aged at 850°C decreases with aging time in the order 1 h > 10 min > 10 h. This result is like the one observed in the impedance analysis.

4. Conclusions

- The increase in the hardness values of the ferrite phase was more pronounced for the samples in the aged condition of 5A steel.
- Potentiodynamic polarization and impedance results showed the beneficial effect of addition of 0.99%pCu and 0.70%pW to the cast SDSS retarding the embrittlement of the 6A steel aged at 850°C for 10 h.
- The characteristic mechanism of pitting corrosion in the aged samples of both materials was selective dissolution of the ferrite phase.
- The capacitance studies using Mott-Schottky's analysis showed that the doping densities for the films formed on the surface of the 6A steel are lower than those observed for the 5A steel.

5. Acknowledgments

We are grateful to the Federal University of Cariri for financial support.

6. References

1. Nilsson JO. Super duplex stainless steels. Mater Sci Technol. 1992;8(8):685-700.
2. Doi T, Adachi T, Kudo T, Usuki N. In situ investigation of CO_2 corrosion in Cr-containing steels in CO_2-saturated salt solution at elevated temperatures and pressures. Corros Sci. 2020;177:108931.
3. Olsson J, Snis M. Duplex - a new generation of stainless steels for desalination plants. Desalination. 2007;205(1-3):104-13.
4. Tavares SSM, Pardal JM, Almeida BB, Mendes MT, Freire JLF, Vidal AC. Failure of superduplex stainless steel flange due to inadequate microstructure and fabrication process. Eng Fail Anal. 2018;84:1-10.
5. Craig B. Clarifying the applicability of PREN equations: a short focused review. Corrosion. 2021;77(4):382-5.
6. Francis R, Byrne G. Duplex stainless steels – alloys for the 21st century. Metals. 2021;11(5):836. https://doi.org/10.3390/met11050836.
7. Sun L, Zhao T, Qiu J, Sun Y, Li K, Zheng H, et al. Point defect model for passivity breakdown on hyper-duplex stainless steel 2707 in solutions containing bromide at different temperatures. Corros Sci. 2021;194:109959.
8. Qiu JH. Passivity and its breakdown on stainless steels and alloys. Surf Interface Anal. 2002;33(10-11):830-33.
9. De Lima HMLF, Bastos IN, Araújo WS, Martins M. Heat treatment effects on ASTM A890/A 890M Gr 5A super duplex stainless steel passivity. Mater Res. 2017;20(2):775-85.
10. Della Rovere CA, Santos FS, Silva RAR, Souza CAC, Kuri SE. Influence of long-term low-temperature aging on the microhardness and corrosion properties of duplex stainless steel. Corros Sci. 2013;68:84-90.
11. Liu H, Sun J, Qian J, Wang B, Shi S, Zhu Y, et al. Revealing the temperature effects on the corrosion behaviour of 2205 duplex stainless steel from passivation to activation in a CO_2-containing geothermal environment. Corros Sci. 2021;187:109495.
12. Ernst P, Newman RC. Pit growth studies in stainless steel foils. II. Effect of temperature, chloride concentration and sulphate addition. Corros Sci. 2002;44:943-54.
13. Wang R. Precipitation of sigma phase in duplex stainless steel and recent development on its detection by electrochemical potentiokinetic reactivation: a review. Corros Commun. 2021;2:41-54.
14. Iacoviello F, Di Cocco V, Franzese E. Integranular corrosion susceptibility analysis in austeno-ferritic (duplex) stainless steels. Fatigue Fract Eng Mater Struct. 2017;4:739-48.
15. Pareige C, Emo J, Saillet S, Domain C, Pareige P. Kinetics of G-phase precipitation and spinodal decomposition in very long aged ferrite of a Mo-free duplex stainless steel. J Nucl Mater. 2015;465:383-9.
16. Hosseini VA, Karlsson L, Wessman S, Fuertes N. Effect of sigma phase morphology on the degradation of properties in a super duplex stainless steel. Materials (Basel). 2018;11(6):933.
17. Gunn RN. Duplex stainless steels: microstructure, properties and applications Cambridge, England: Abington Publishing; 1997.
18. Chun EJ, Baba H, Nishimoto K, Saida K. Precipitation of sigma and chi phases in δ-ferrite of Type 316FR weld metals. Mater Charact. 2013;86:152-66.
19. Tavares SSM, Da Silva MR, Neto JM. Magnetic property changes during embrittlement of a duplex stainless steel. J Alloys Compd. 2000;313:168-73.
20. Lee J, Kim I, Kimura A. Application of small punch test to evaluate sigma-phase embrittlement of pressure vessel cladding material. J Nucl Sci Technol. 2003;40(9):664-71.
21. Ujiro T, Satoh S, Staehle RW, Smyrl WH. Effect of alloying Cu on the corrosion resistance of stainless steels in chloride media. Corros Sci. 2001;43(11):2185-200.
22. Hermas AA. Effects of alloying additions on corrosion and passivation behaviors of type 304 stainless steel. Corrosion. 1995;1(51):3-10.
23. Oguzie EE, Li J, Liu Y, Chen D, Li Y, Yang K, et al. The effect of Cu addition on the electrochemical corrosion and passivation behavior of stainless steels. Electrochim Acta. 2010;55(17):5028-35.
24. De Lima HMLF, Tavares SSM, Bastos IN, Araújo WS, Martins M. Corrosion Resistance of Cu-Alloyed Precipitation Hardenable Duplex Stainless Steel ASTM A890 Grade 1B. Mater Res. 2019;22(1)
25. De Lima HMLF, Tavares SSM, Araújo WS, Martins M. The effect of copper addition on the corrosion resistance of cast duplex stainless steel. J Mater Res Technol. 2019;8(2):2107-19.
26. Adhitya K, Thillairajan K, Shankar RD. Phase stability study on wrought duplex and super duplex stainless steels grade 4A, 5A and 6A at elevated temperatures and the effect on their mechanical properties. AIP Conf Proc. 2019;2128(1):1-13.
27. Hsieh CC, Wu W. Overview of intermetallic sigma phase precipitation in stainless steels. ISRN Metallurgy. 2012;1-16.
28. Charles J. Super duplex stainless steels: structure and properties. In: Conference on Duplex Stainless Steels on DSS '91; 1991; Les Ulis. Proceedings. Les Ulis, France: Les Editions de Physique; 1991. p. 3-48.
29. Wegrzyn J, Klimpel A. The effect of alloying elements on sigma phase formation in 18-8 weld metals. Weld J. 1981;60(8):146s-54s.
30. Stradomski Z, Dyja D. Sigma phase precipitation in duplex phase stainless steel. Sci Res. 2009;3:17-8.
31. Silva DDS, Lima LSDC, Araújo A, Silva VD. The effect of microstructural changes on mechanical and electrochemical corrosion properties of duplex stainless steel aged for short periods. Materials (Basel). 2020;13(23):1-13.
32. Magnabosco R, Alonso-Falleiros N. Pit morphology and its relation to microstructure of 850°C aged duplex stainless steel. Corrosion. 2005;61(2):130-6.
33. Wolynec S, Alonso-Falleiros N, Hakim A. Comparison between potentiodynamic and potentiostatic tests for pitting potential measurement of duplex stainless steels. Corrosion. 1999;55(5):443-8.
34. Moayed MH, Newman RC. Evolution of current transients and morphology of metastable and stable pitting on stainless steel near the critical pitting temperature. Corros Sci. 2006;48:1004-18.
35. Magnabosco R, Morais L, Dos Santos DC. Use of composition profiles near sigma phase for assessment of localized corrosion resistance in a duplex stainless steel. Calphad. 2019;64:126-30.
36. Sedriks AJ. Corrosion of stainless steels. 2nd ed. New York: John Wiley & Sons; 1996.
37. Jeon SH, Kim ST, Lee IS, Kim JS, Kim KT, Park YS. Effects of W substitution on the precipitation of secondary phases and the associated pitting corrosion in hyper duplex stainless steels. J Alloys Compd. 2012;544(15):166-72.
38. Jeon SH, Kim ST, Lee IS, Kim JS, Kim KT, Park YS. Effects of Cu on the precipitation of intermetallic compounds and the intergranular corrosion of hyper duplex stainless steels. Corros Sci. 2013;66:217-24.
39. Tavares SSM, Pardal JM, Almeida BB, Mendes MT, Freire JLF, Vidal AC. Failure of superduplex stainless steel flange due to inadequate microstructure and fabrication process. Eng Fail Anal. 2018;84:1-10.
40. Silva DDS, Simoes TA, Macedo DA, Bueno AHS, Torres SM, Gomes RM. Microstructural influence of sigma phase on pitting corrosion behavior of duplex stainless steel/NaCl electrolyte couple. Mater Chem Phys. 2021;259(1):124056.
41. Wang J, Chen WL, Meng HJ, Cui YS. Influence of sigma phase on corrosion and mechanical properties of 2707 hyper-duplex stainless steel aged for short periods. J Iron Steel Res Int. 2019;26(5):452-61.

42. Azevedo CRF, Pereira HB, Wolynec S, Padilha AF. An overview of the recurrent failures of duplex stainless steels. Eng Fail Anal. 2019;97:161-88.
43. Markhali BP, Naderi R, Mahdavian M, Sayebani M, Arman SY. Electrochemical impedance spectroscopy and electrochemical noise measurements as tool to evaluate corrosion inhibition of azole compounds on stainless steel in acidic media. Corros Sci. 2013;75:269-79.
44. Walter GW. A review of impedance plot methods used for corrosion performance analysis of painted metals. Corros Sci. 1986;26(9):681-703.
45. Li J, Xie F, Wang D, Ma C, Wu M, Gong K. Effect of magnetic field on stress corrosion cracking induced by Sulfate-reducing bacteria. Constr Build Mater. 2021;303:124521.
46. Brug GJ, Eeden ALG, Sluyters-Rehbach M, Sluyters JH. The analysis of electrode impedances complicated by the presence of a constant phase element. J Electroanal Chem Interfacial Electrochem. 1984;176:275-95.
47. Popova A, Raicheva S, Sokolova E, Christov M. Frequency dispersion of the interfacial impedance at mild steel corrosion in acid media in the presence of benzimidazole derivatives. Langmuir. 1996;12:2083-9.
48. Popova A, Raicheva S, Sokolova E, Christov M. AC and DC study of the temperature effect on mild steel corrosion in acid media in the presence of benzimidazole derivatives. Corros Sci. 2003;45:33-58.
49. Bentiss F, Jama C, Mernari B, El Attari H, El Kadi L, Lebrini M, et al. Corrosion control of mild steel using 3,5-bis(4-methoxyphenyl)-4-amino-1,2,4-triazole in normal hydrochloric acid medium. Corros Sci. 2009;51:1628-35.
50. Zahrani EM, Saatchi A, Alfantazi A. Pitting of 316L stainless steel in flare piping of a petrochemical plant. Eng Fail Anal. 2010;17:810-7.
51. Di Paola A. Semiconducting properties of passive films on stainless steels. Electrochim Acta. 1989;34:203-10.
52. Fattah-Alhosseini A, Soltani F, Shirsalimi F, Ezadi B, Attarzadeh N. The semiconducting properties of passive films formed on AISI 316 L and AISI 321 stainless steels: a test of the point defect model (PDM). Corros Sci. 2011;53:3186-92.
53. Hakiki NE, Rondot SB, Belo MC. The electronic structure of passive films formed on stainless steels. Corros Sci. 1995;37(11):1809-22.
54. Montemor MF, Ferreira MGS, Hakiki NE, Da Cunha Belo M. Chemical composition and electronic structure of the oxide films formed on 316L stainless steel and nickel based alloys in high temperature aqueous environments. Corros Sci. 2000;42:1635-50.
55. Kang J, Yang Y, Xi J, Shao H. Semiconducting properties of passive films formed on electroplated Ni and Ni–Co alloys. Corros Sci. 2008;50:3576-80.
56. Alves VA, Brett CMA. Characterisation of passive films formed on mild steels in bicarbonate solution by EIS. Electrochim Acta. 2002;47:2081-90.